Light & Matter (part 2)

Semiclassical approach to atom-light interactions

Atoms: hydrogen and hydrogen-like (alkali)

main structure

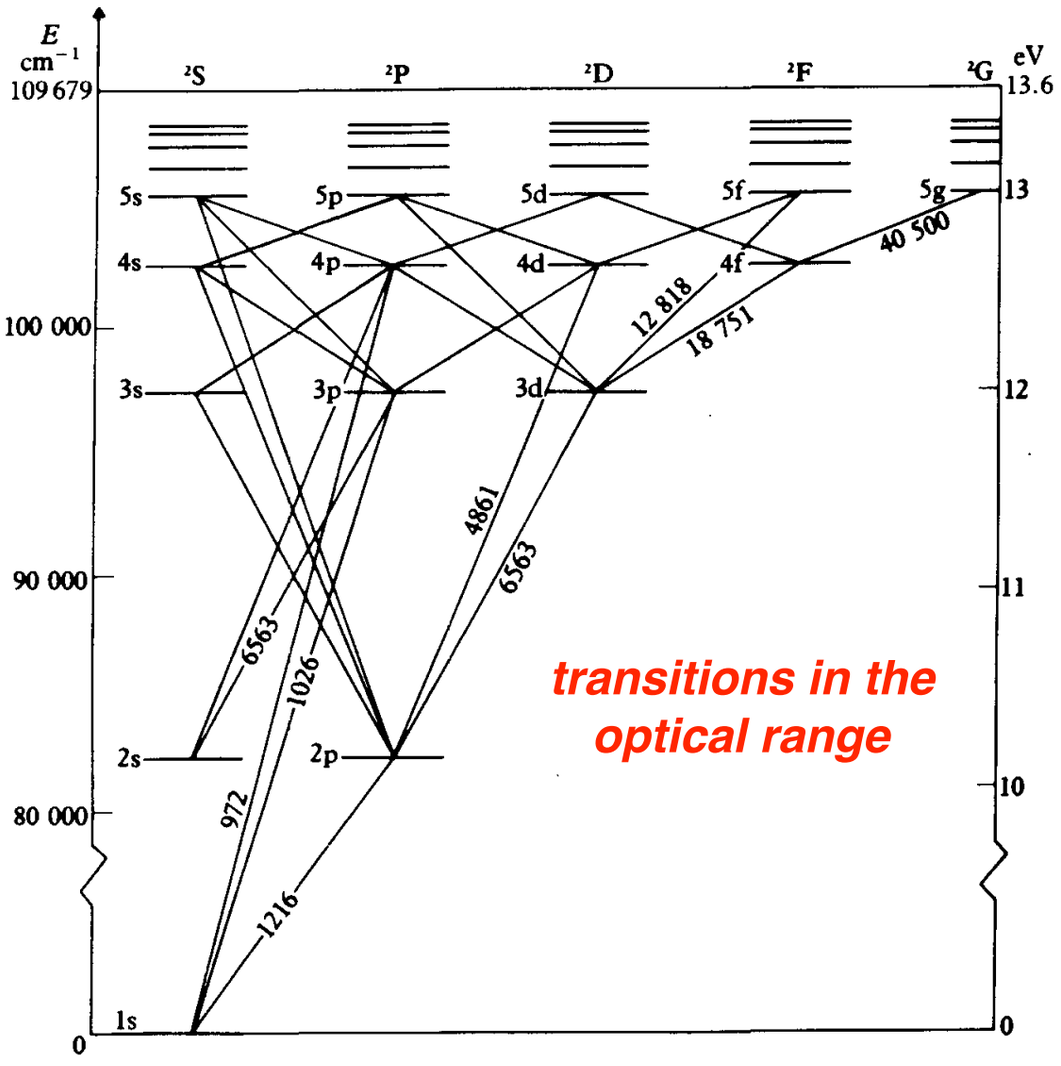

4.4 Term, or Grotrian diagram for atomic hydrogen. The ordinate shows the energy above the 1s ground state in cm^{-1} ($8065\ cm^{-1} \equiv 1$ eV) on the left and in eV on the right and the energy levels are shown plotted against the orbital angular momentum. Transitions obeying the $\Delta l = \pm 1$ selection rule are indicated by solid lines. The numbers against the lines indicate the wavelength in angström units ($1\ Å \equiv 10^{-8}$ cm). For clarity, only transitions between the lower-lying levels are shown, and the wavelengths are shown only for a selection of lines. The splitting due to fine structure is too small to be shown on a diagram of this scale.

transitions in the optical range

fine, hyperfine structure and Lamb shift

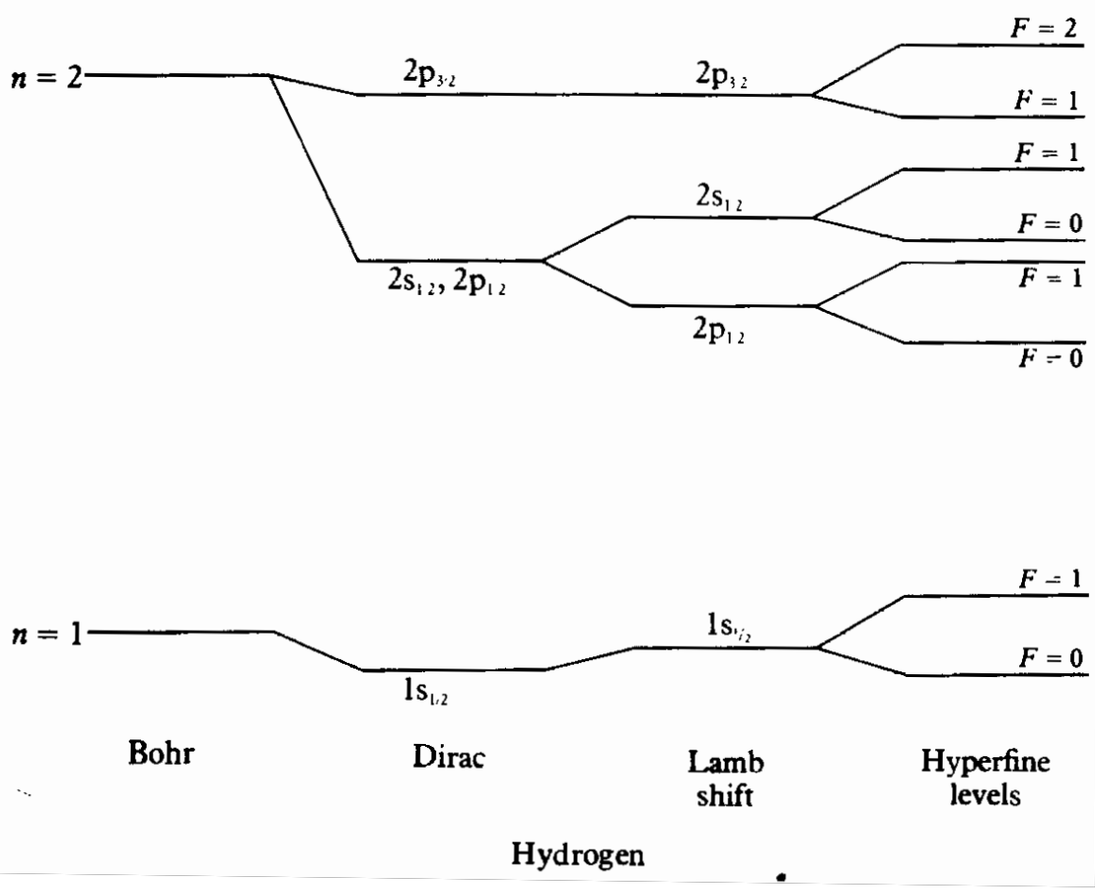

optical cavities

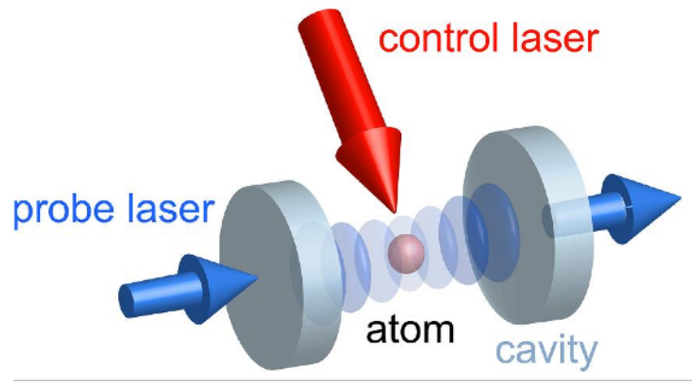

Brandsen & Joachain: *Physics of Atoms and Molecules* (2003)

Artificial atoms: quantum dots

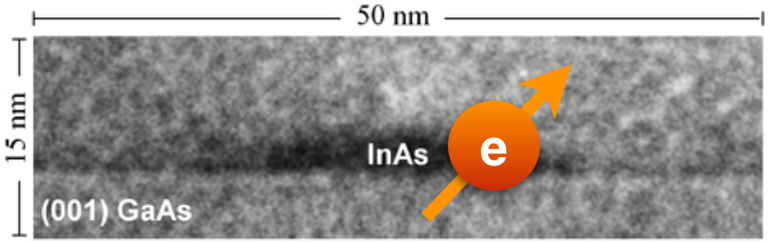

semiconductor heterostructures
(InAs islands in a GaAs matrix)

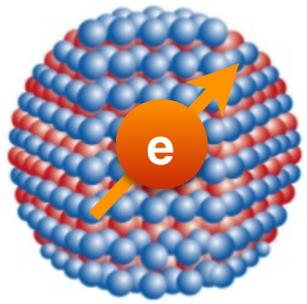

semicond. nanocrystals

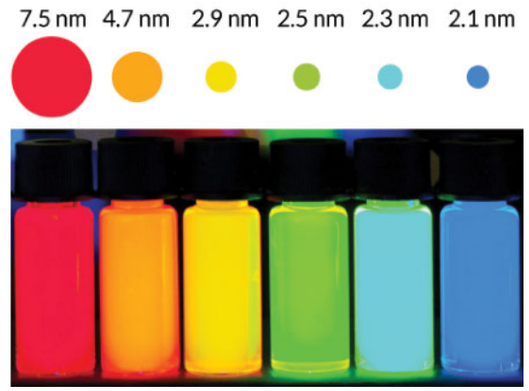

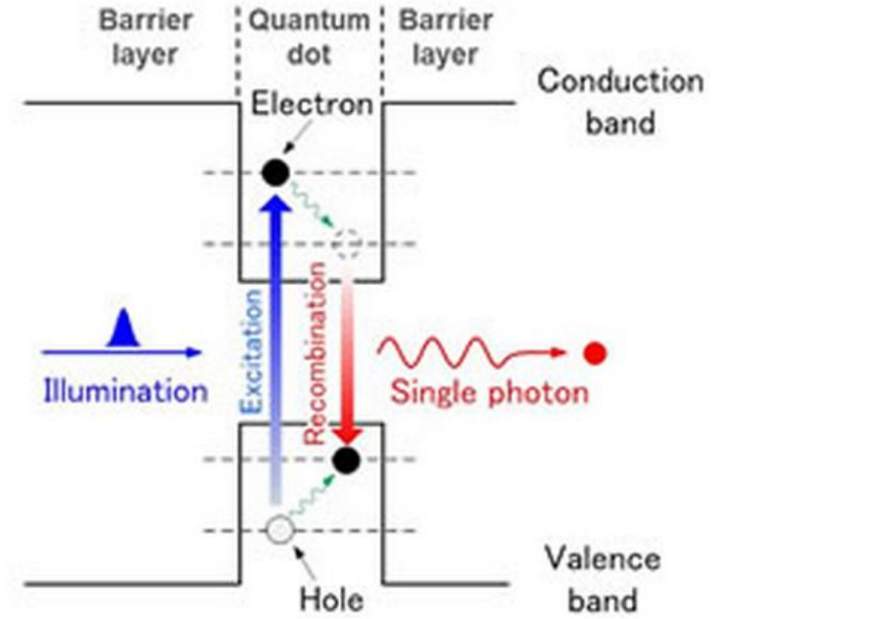

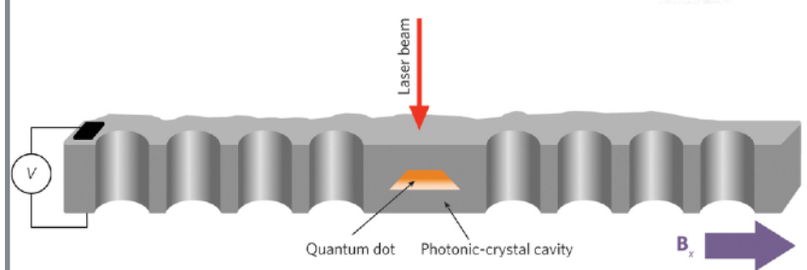

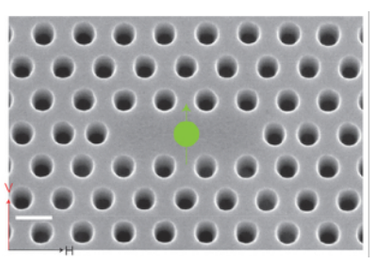

photonic crystal cavity

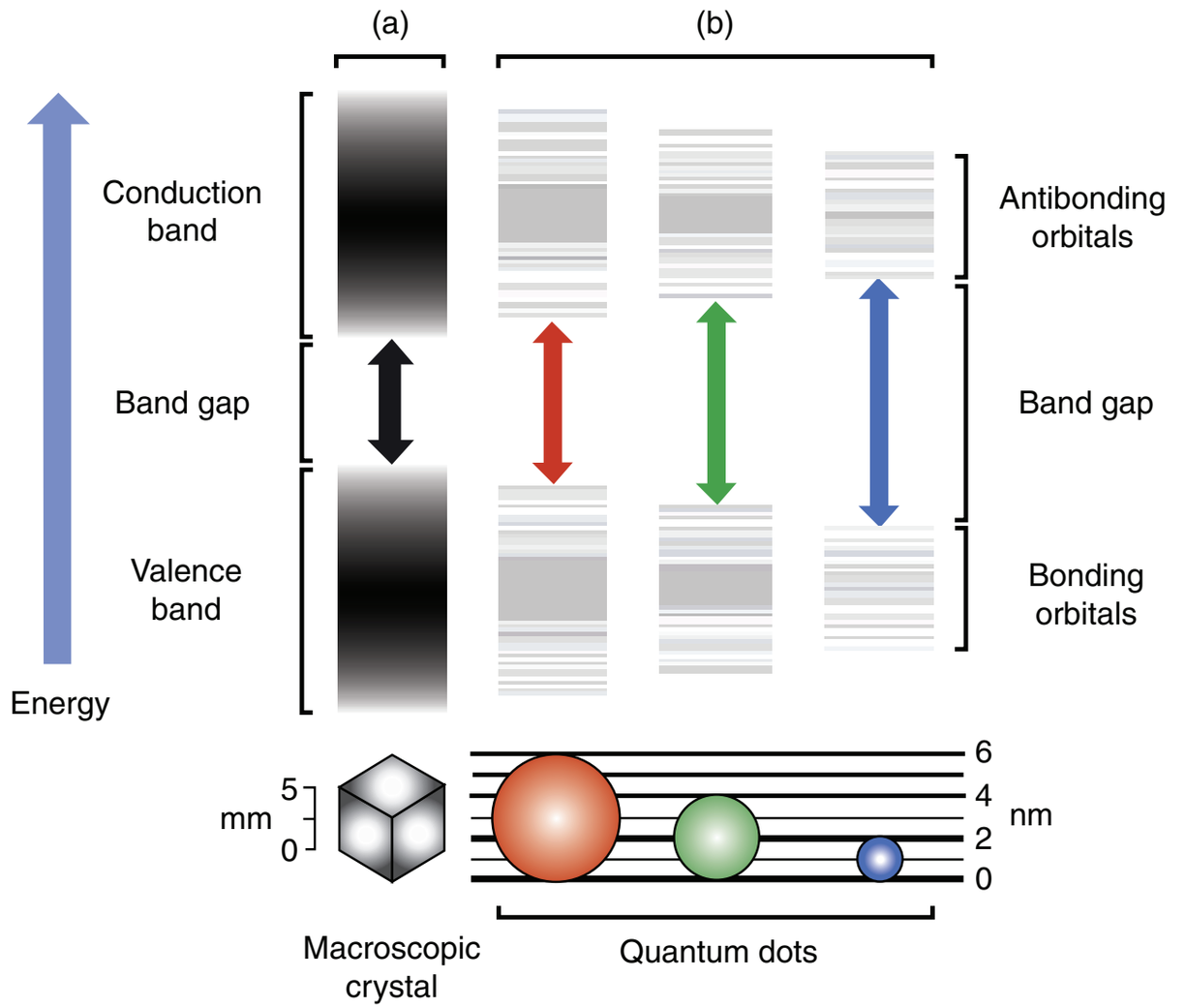

Artificial atoms: quantum dots

Electrically defined QD

a

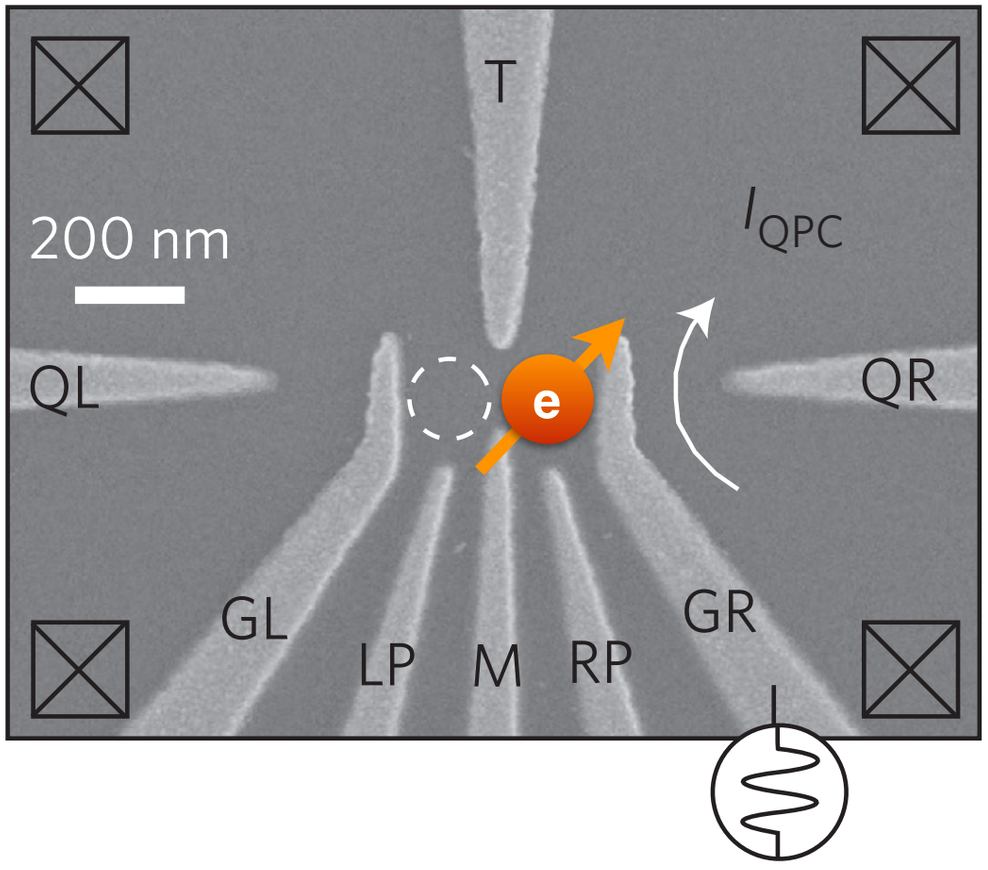

microwave source

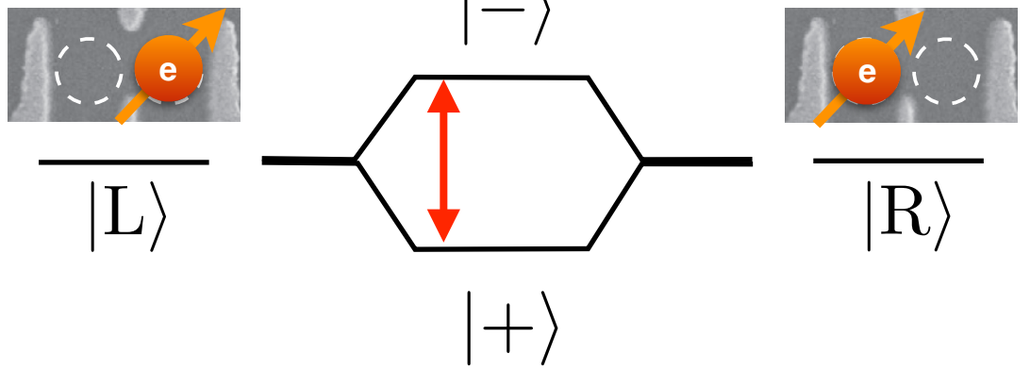

nature nanotechnology

LETTERS

PUBLISHED ONLINE: 16 FEBRUARY 2015 | DOI: 10.1038/NNANO.2014.336

Microwave-driven coherent operation of a semiconductor quantum dot charge qubit

Dohun Kim[1], D. R. Ward[1], C. B. Simmons[1], John King Gamble[2], Robin Blume-Kohout[2], Erik Nielsen[2], D. E. Savage[3], M. G. Lagally[3], Mark Friesen[1], S. N. Coppersmith[1] and M. A. Eriksson[1]*

Artificial atoms: superconducting circuits (qubits)

Cooper-pair box

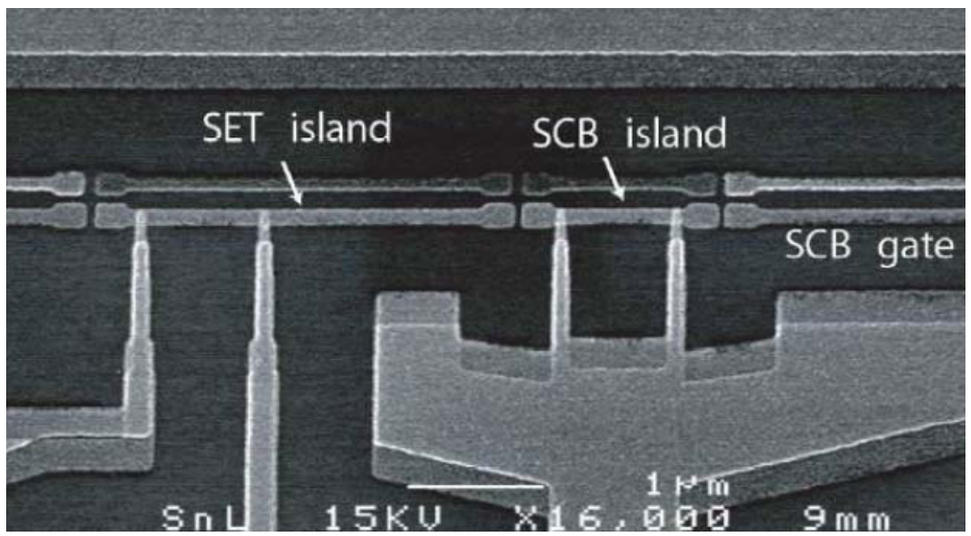

$$H = E_c \sum_n (n - n_g)^2 \, |n\rangle\langle n| - E_J \sum_n (|n\rangle\langle n+1| + \text{h.c.})$$

$$E_c = \frac{q^2}{2C} = \frac{(2e)^2}{2C}$$

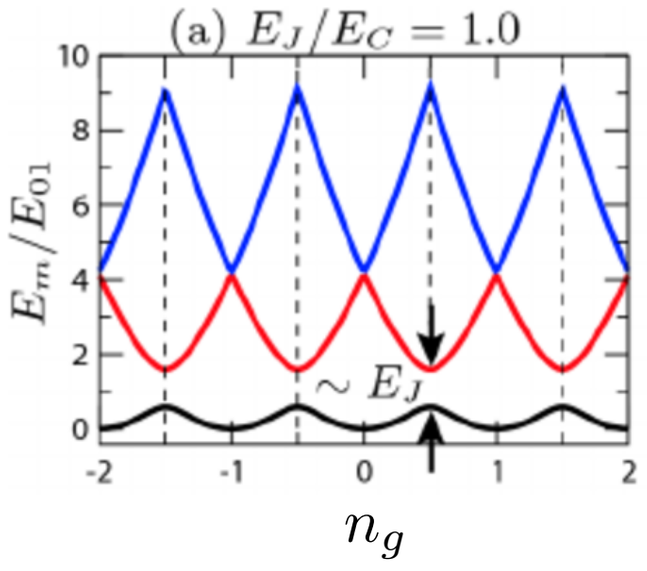

qubit in a ***microwave cavity***

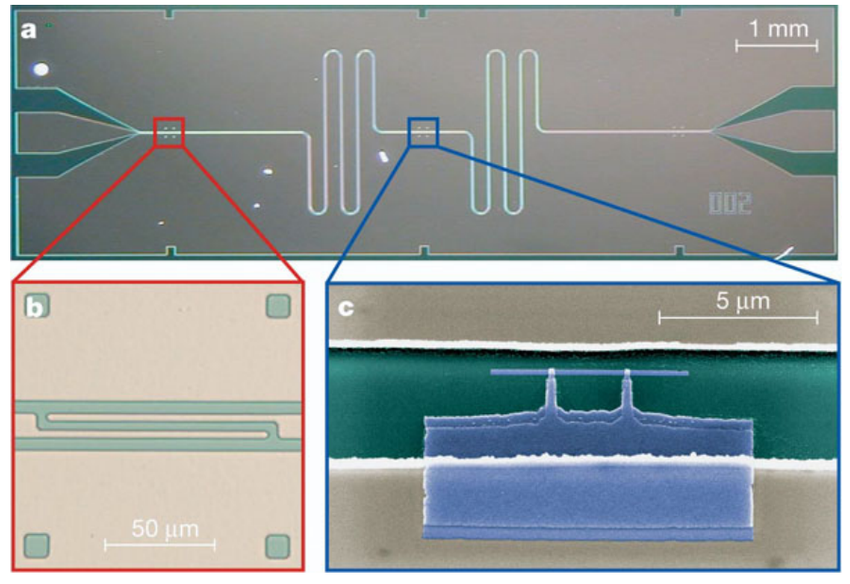

A. Wallraf et al., Nature 2004

Rabi oscillations - single Rb atom

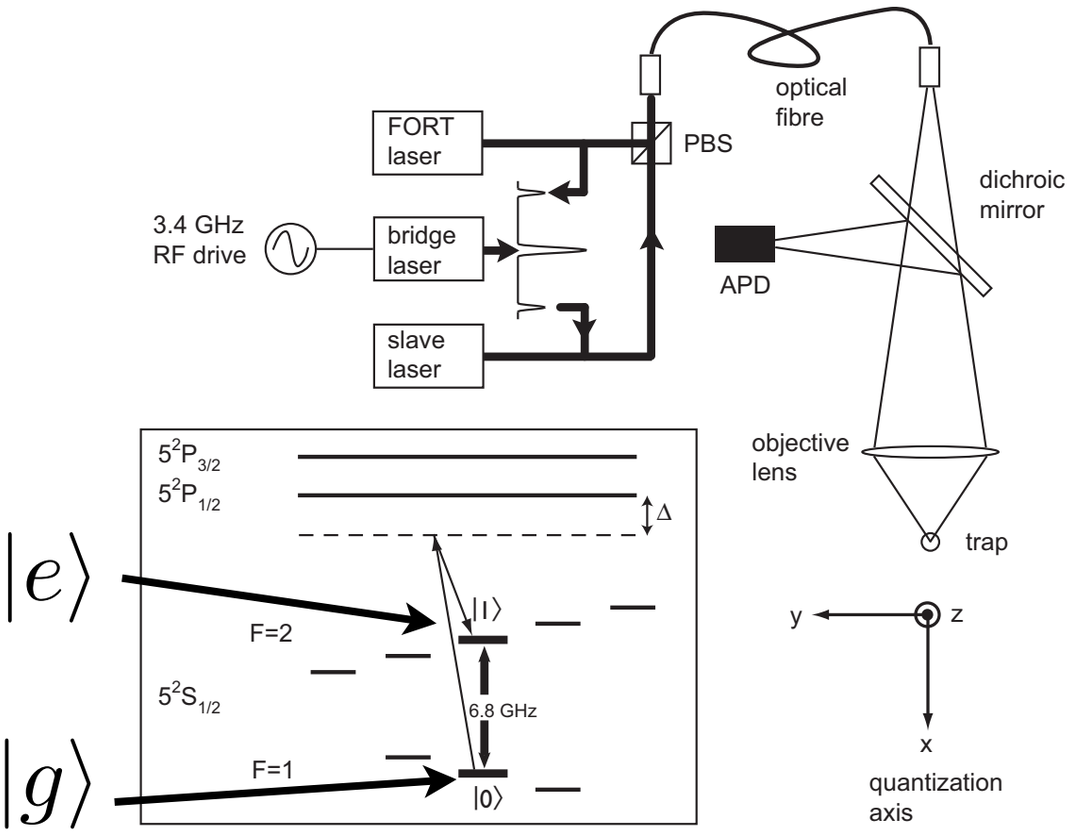

FIG. 1: Experimental setup. A high performance objective lens creates a tightly focussed optical dipole trap, which also acts as one of the Raman beams. The second Raman beam is generated using two additional diode lasers, and is superimposed with the trapping beam on a polarising beam splitter (PBS). A single polarization-maintaining fibre carries both beams to the experiment. Inset shows the relevant energy levels of ^{87}Rb. The quantisation axis is defined by a 0.36 mT magnetic field along the x-axis.

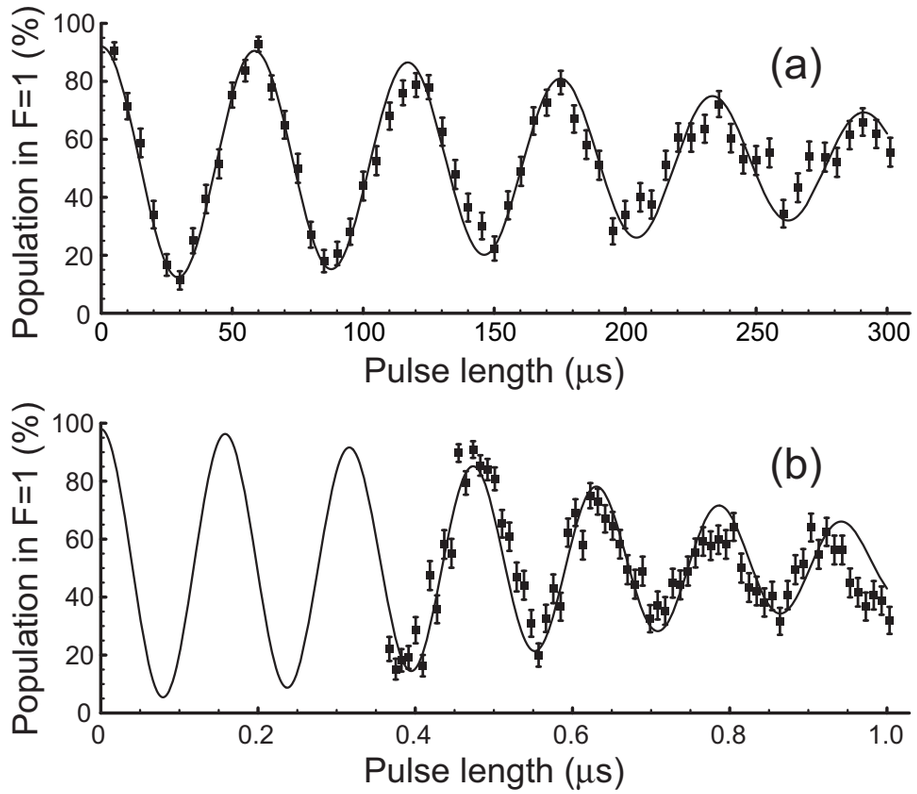

FIG. 2: Single-atom Rabi oscillations. We measure the fraction of atoms in $F = 1$ as a function of the Raman pulse length, at low (a) and high (b) intensity. We observe damped Rabi oscillations between the two qubit states with Rabi frequencies of $\Omega = 2\pi \times 18$ kHz (a) and $\Omega = 2\pi \times 6.7$ MHz (b). In (b) we could not observe the first 400 ns due to the response time of the acousto-optic modulator. The error bars correspond to the quantum projection noise.

M. P. A. Jones et al., Phys. Rev. A 75, 040301(R) (2007)

P. Grangier's group, Institut d'optique - Palaiseau

Atomic clocks - Cs beams

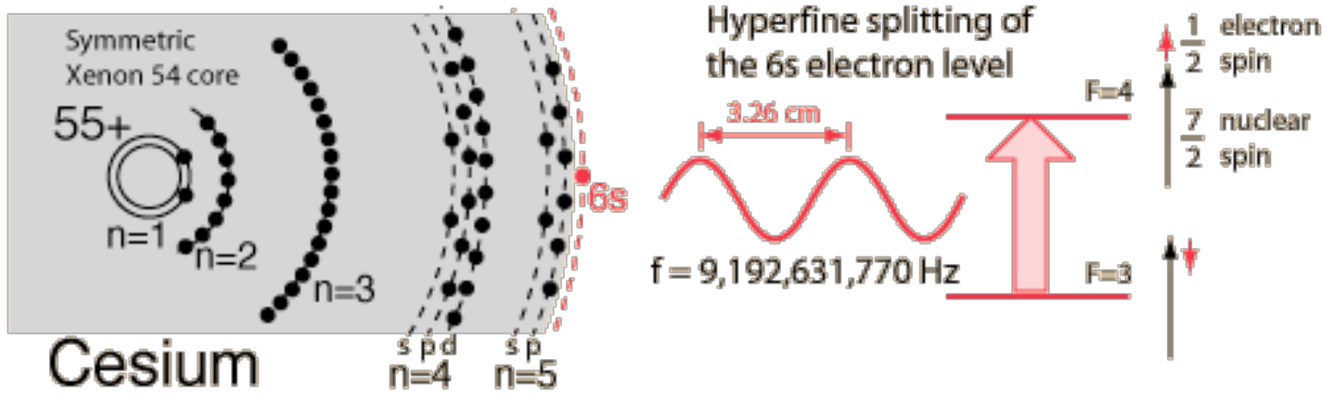

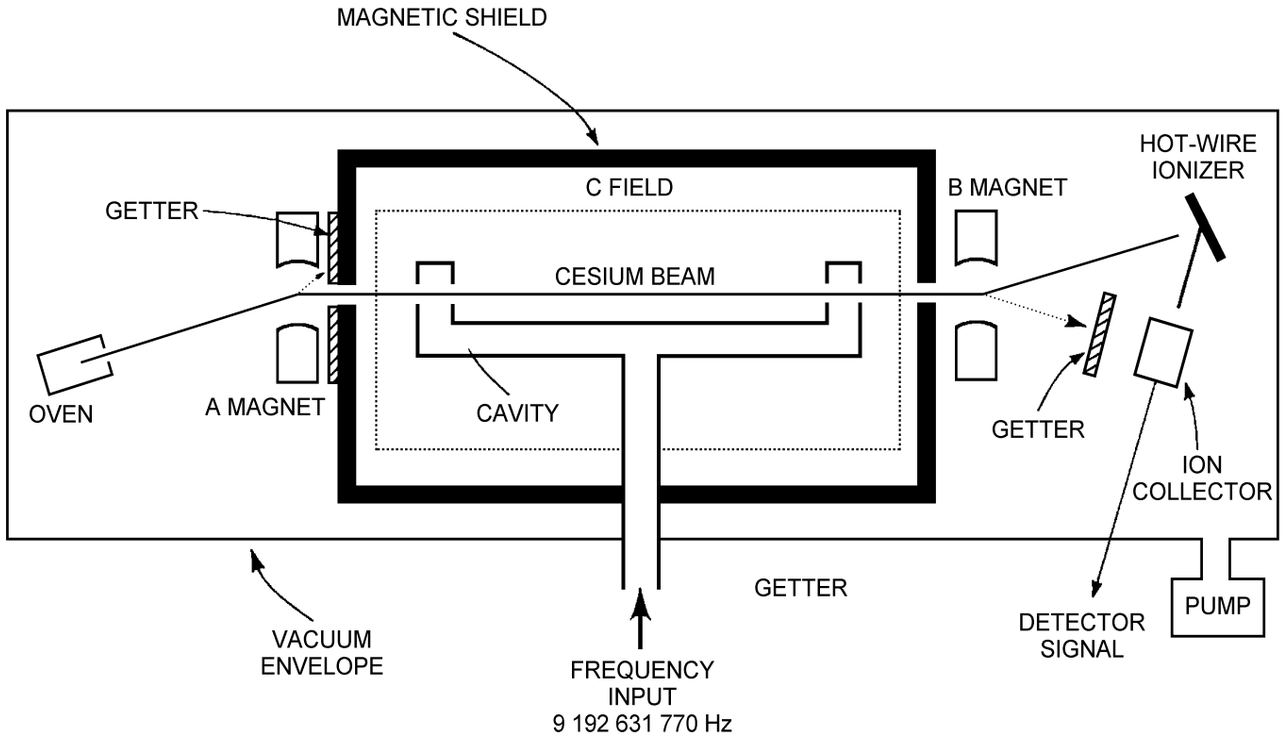

Fig. 1. Diagram of a cesium-beam frequency standard using magnetic state selection and detection. The form of Ramsey interrogation involves a U-shaped microwave cavity, called a Ramsey cavity, where the oscillatory fields are spatially separated.

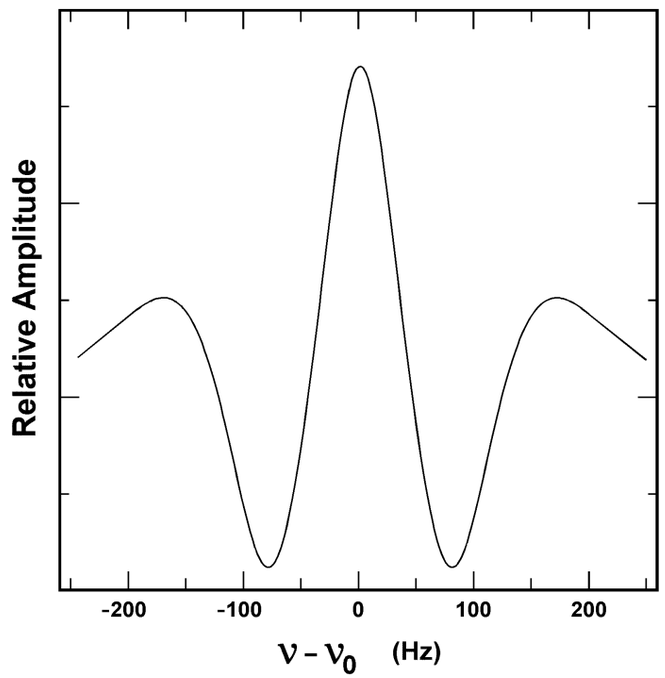

Fig. 2. NIST-7 Ramsey pattern ($F = 3 \leftrightarrow F = 4$) transition in the ground state). The central fringe has a full linewidth at half maximum of about 65 Hz.

Atomic clocks - Cs atomic fountain

Atomic fountain

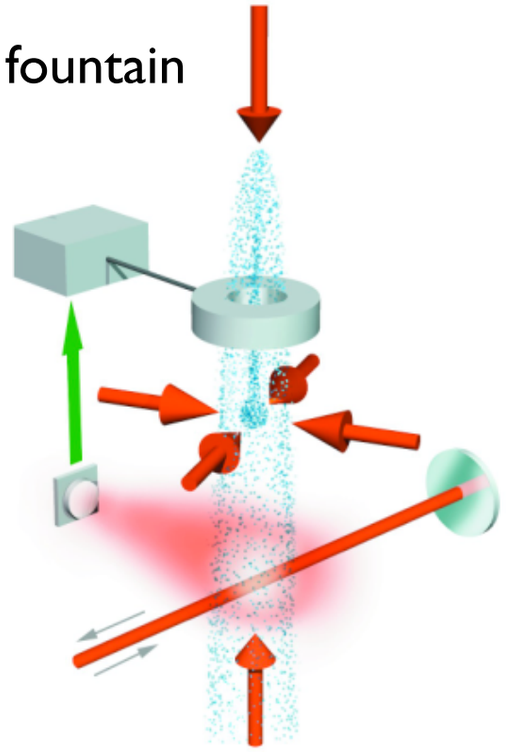

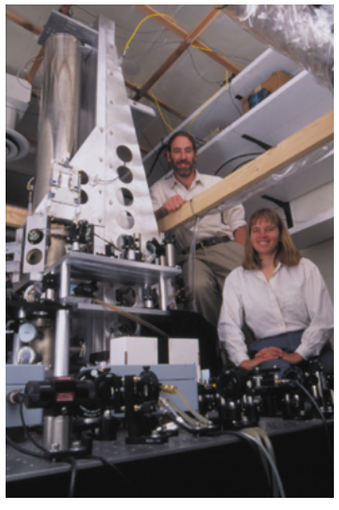

NIST - Boulder, CO (USA)
NIST - F1 / NIST - F2

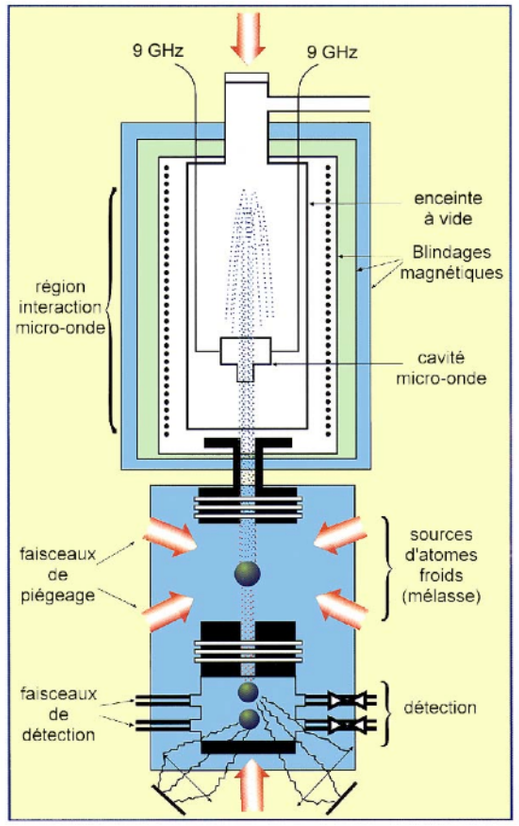

Observatoire de Paris
(France)

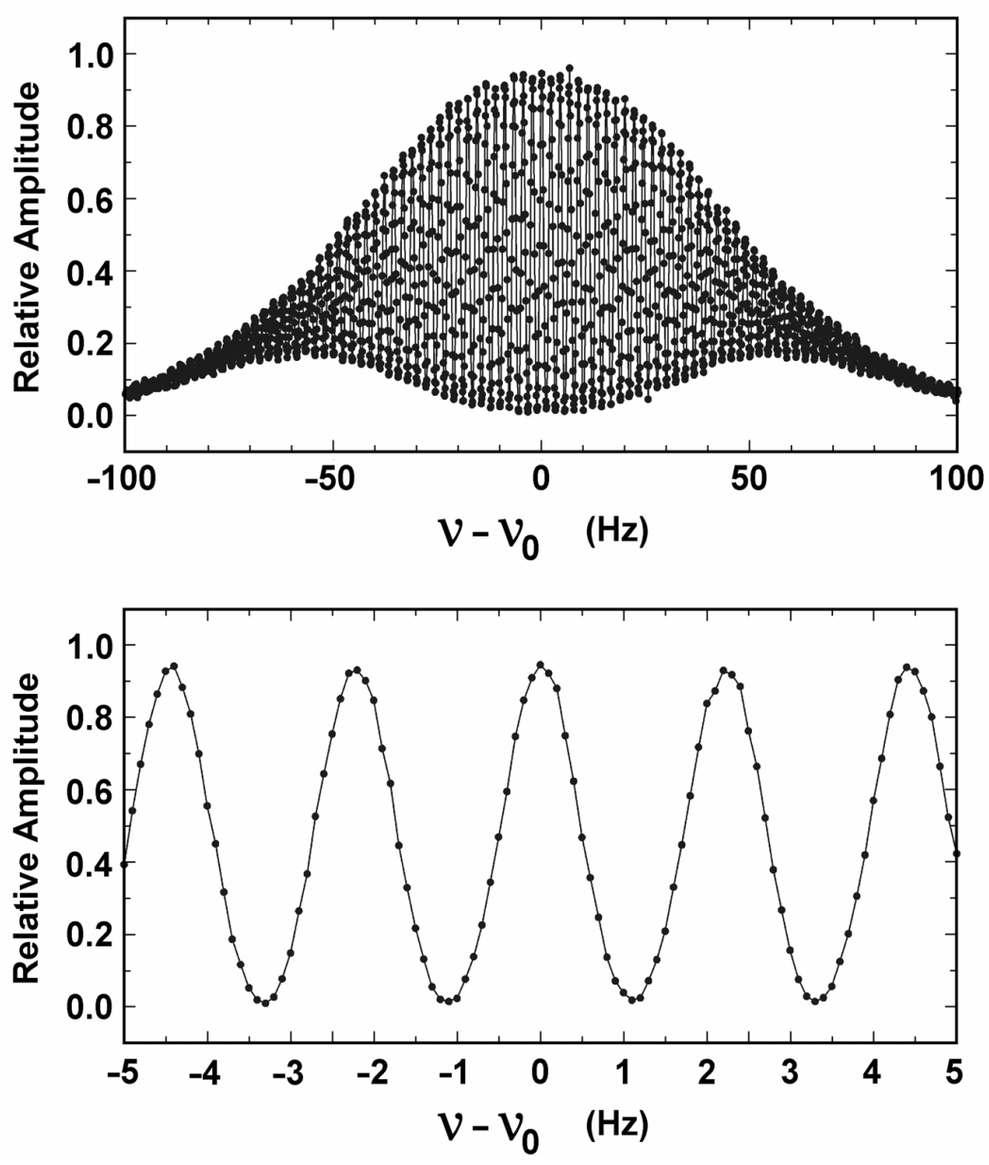

Fig. 4. NIST-F1 Ramsey pattern. The upper portion of the figure shows the entire ground state ($F = 3 \leftrightarrow F = 4$) pattern, while the lower portion of the figure shows an expanded view of the central fringe. The full linewidth at half maximum is about 1 Hz.

Ramsey fringes

Rabi & Ramsey

The Nobel Prize in Physics 1944

Isidor Isaac Rabi
Prize share: 1/1

The Nobel Prize in Physics 1944 was awarded to Isidor Isaac Rabi *"for his resonance method for recording the magnetic properties of atomic nuclei"*.

The Nobel Prize in Physics 1989

Norman F. Ramsey
Prize share: 1/2

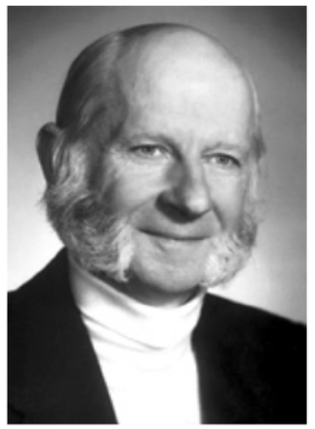

Hans G. Dehmelt
Prize share: 1/4

Wolfgang Paul
Prize share: 1/4

The Nobel Prize in Physics 1989 was divided, one half awarded to Norman F. Ramsey *"for the invention of the separated oscillatory fields method and its use in the hydrogen maser and other atomic clocks"*, the other half jointly to Hans G. Dehmelt and Wolfgang Paul *"for the development of the ion trap technique"*.

Sub-Doppler cooling

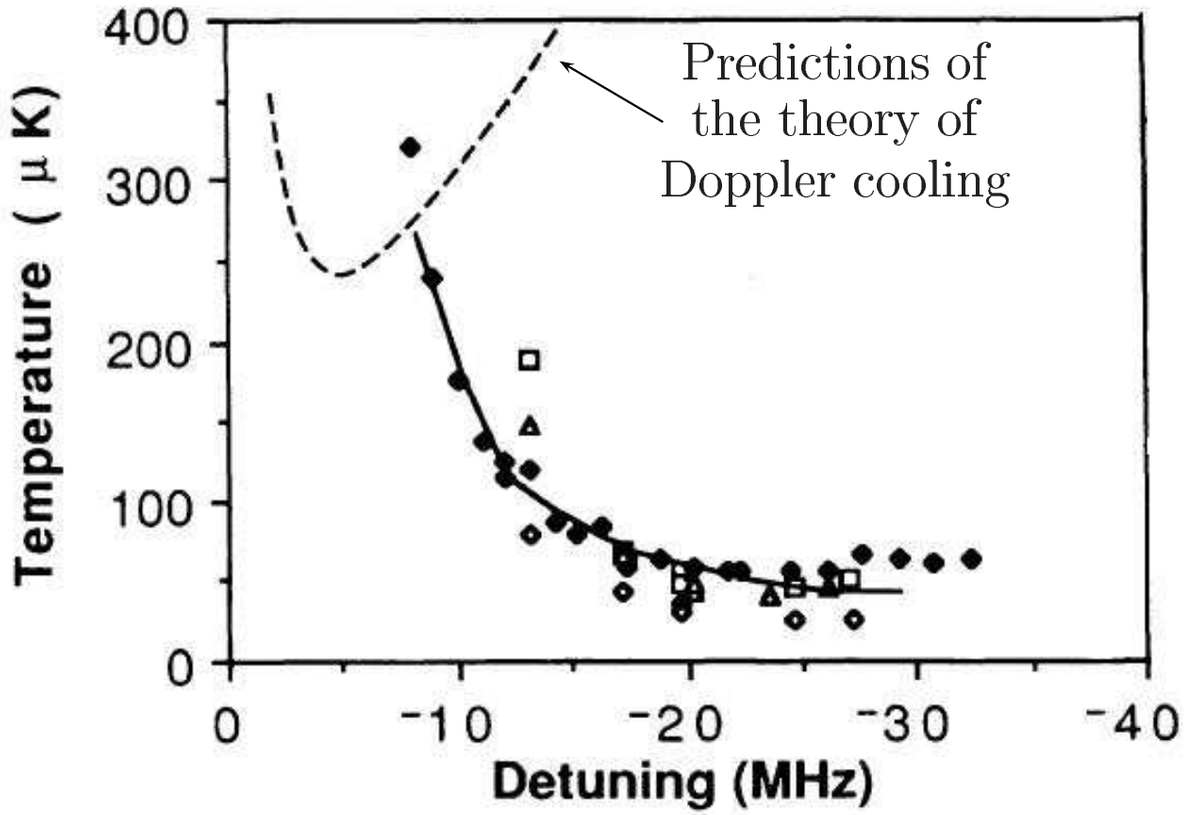

Fig. 13.2 Example of experimental results obtained by the time-of-flight method. The variations with the detuning of the measured temperatures (data points and solid line) are not in agreement with the prediction deduced from the theory of Doppler cooling (dashed curve). The temperatures are much lower than expected and do not pass through a minimum when the detuning is increased. Figure adapted from [Lett *et al.* (1988)]. Copyright: American Physical Society.

Magneto-optical trap (MOT)

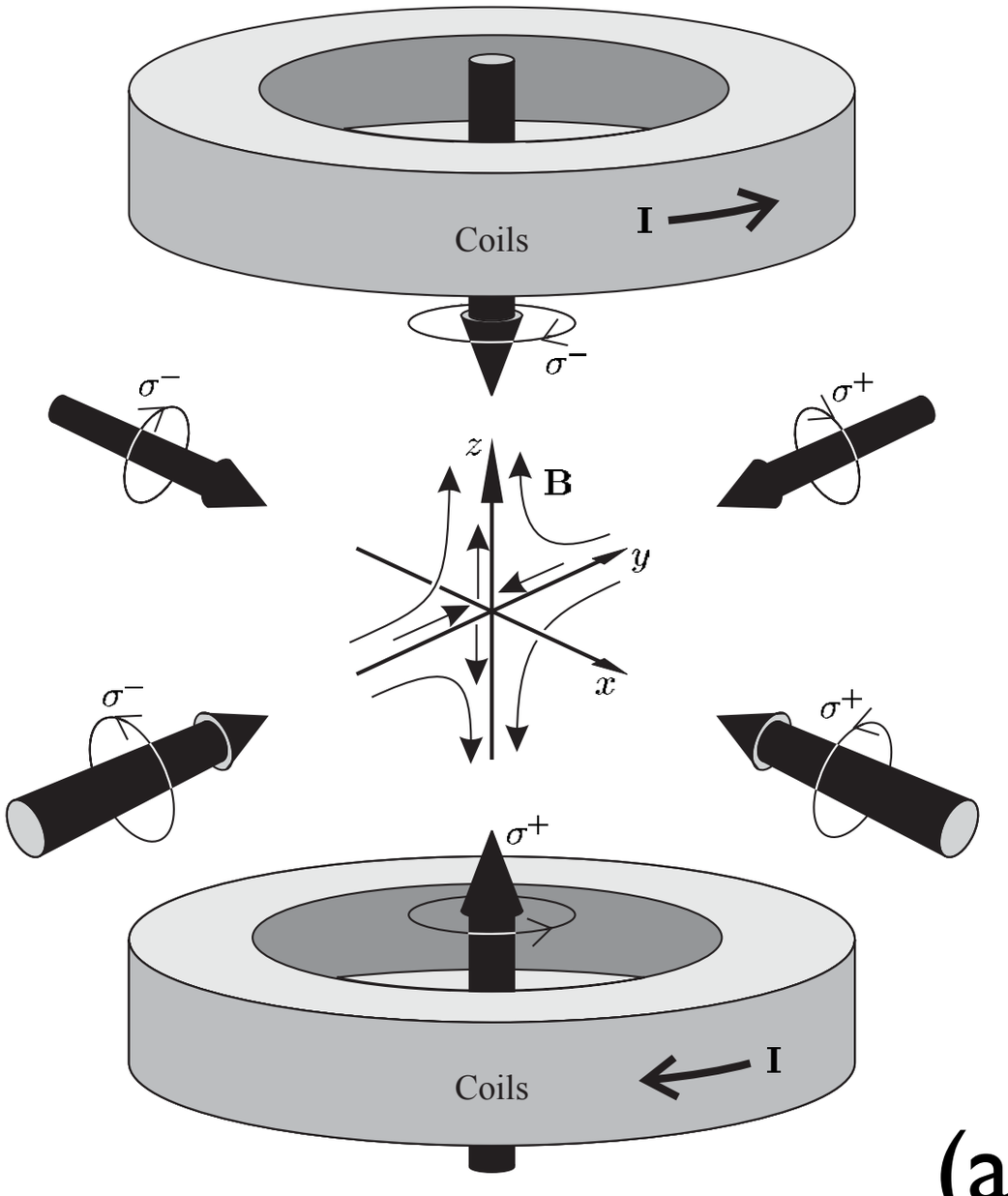

(a)

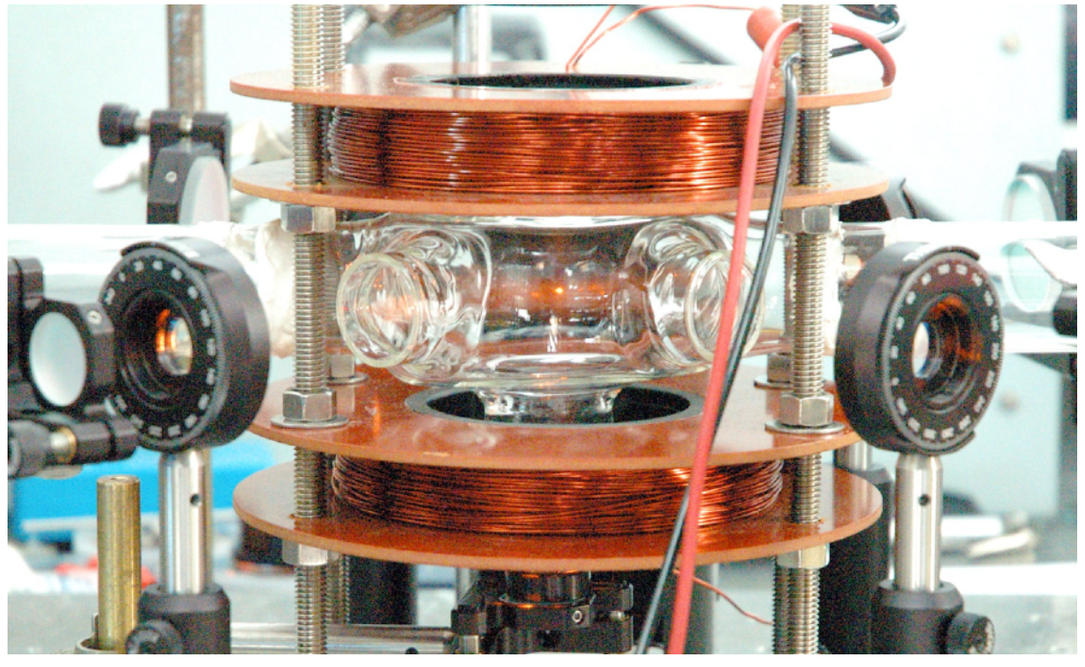

(b)

From laser cooling to BEC

The Nobel Prize in Physics 1997

Steven Chu
Prize share: 1/3

Claude Cohen-Tannoudji
Prize share: 1/3

William D. Phillips
Prize share: 1/3

The Nobel Prize in Physics 1997 was awarded jointly to Steven Chu, Claude Cohen-Tannoudji and William D. Phillips *"for development of methods to cool and trap atoms with laser light"*.

The Nobel Prize in Physics 2001

Eric A. Cornell
Prize share: 1/3

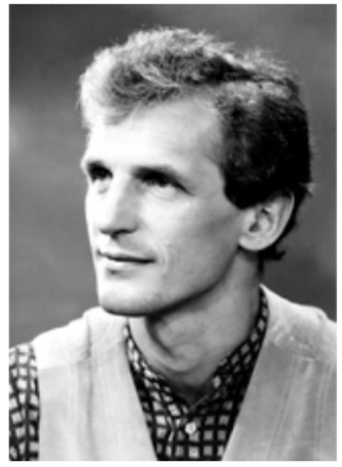

Wolfgang Ketterle
Prize share: 1/3

Carl E. Wieman
Prize share: 1/3

The Nobel Prize in Physics 2001 was awarded jointly to Eric A. Cornell, Wolfgang Ketterle and Carl E. Wieman *"for the achievement of Bose-Einstein condensation in dilute gases of alkali atoms, and for early fundamental studies of the properties of the condensates"*.

Linear Paul trap for ions

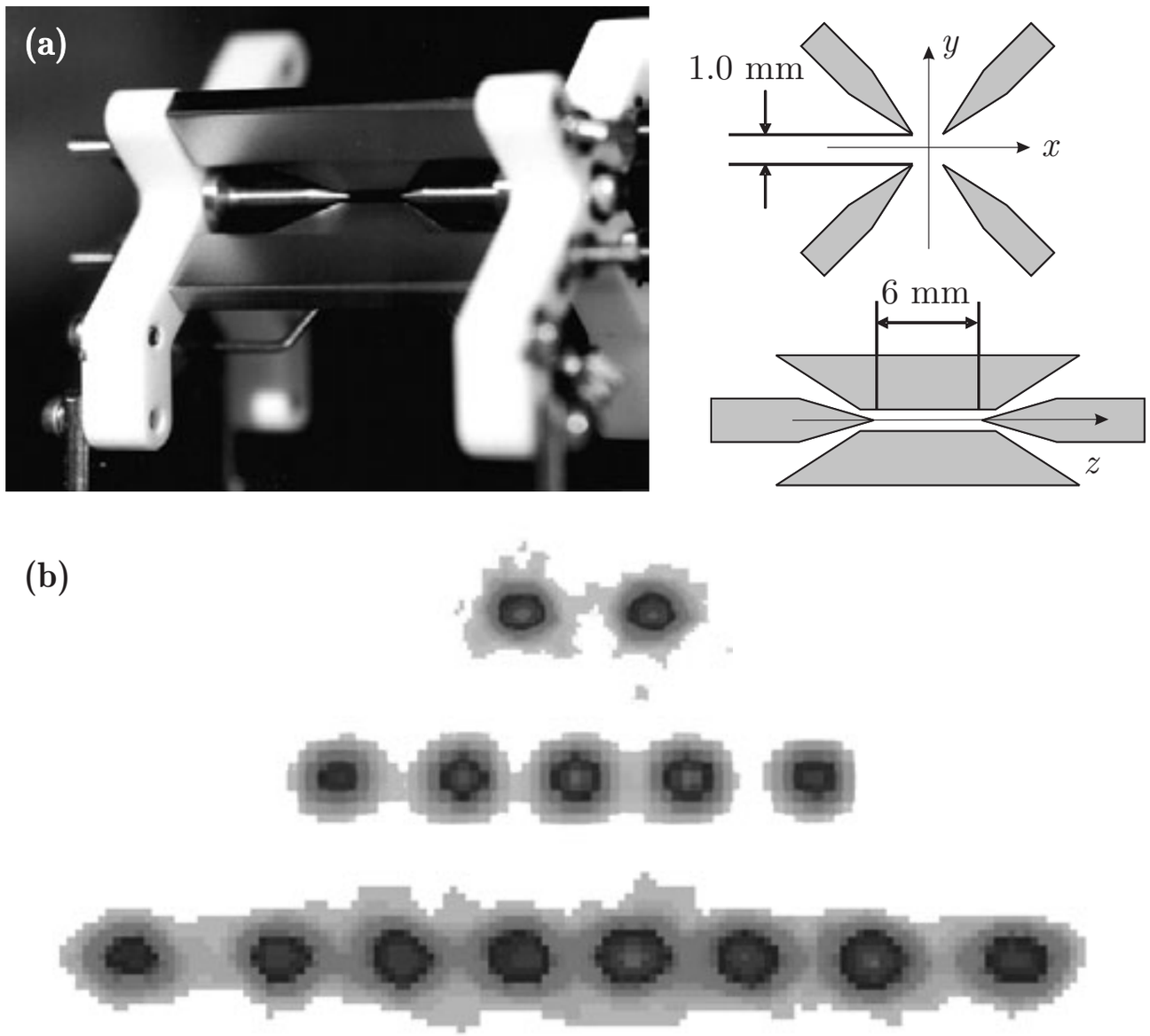

Fig. 8.3 Linear ion trap. (a) Photograph of the actual trap, together with a scheme of the electrode configuration. (b) Linear strings of two, five and eight ions in the trap. Courtesy of R. Blatt.

Coulomb crystals in Paul traps

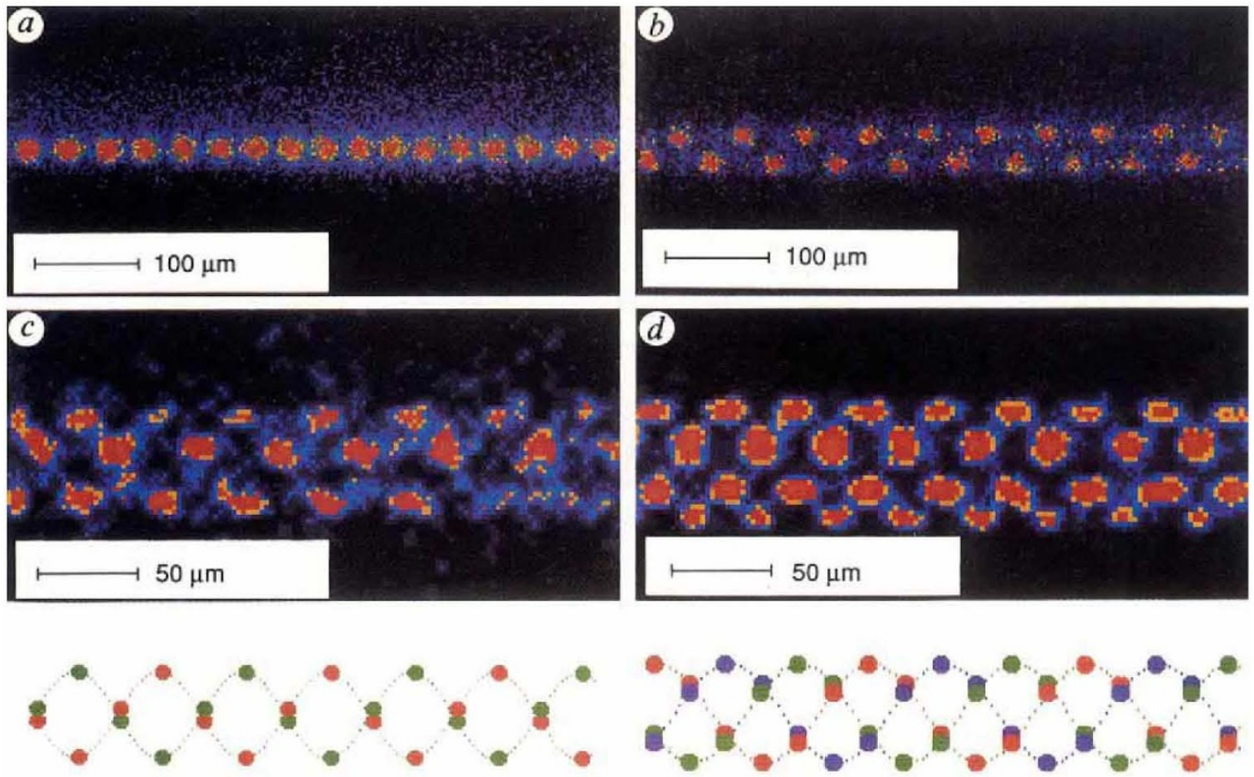

FIG. 2 Colour-coded images of crystalline structures of laser-cooled $^{24}Mg^{+}$ ions. The intensity increases from violet to blue, yellow and red. Individual ions could be resolved in these images. The ions arrange themselves in minimum energy configurations. *a*, For low ion density ($\lambda = 0.29$) the ions form a string along the field axis; *b*, increasing the ion density changes the configuration to a zig-zag ($\lambda = 0.92$). At still higher ion densities the ions form ordered helical structures on the surface of a cylinder: *c*, two interwoven helices at $\lambda = 1.9$; *d*, three interwoven helices at $\lambda = 2.6$. Experimental images are displayed above, visualizations below.

G. Birkl et al., Nature 357, 310 (1992)

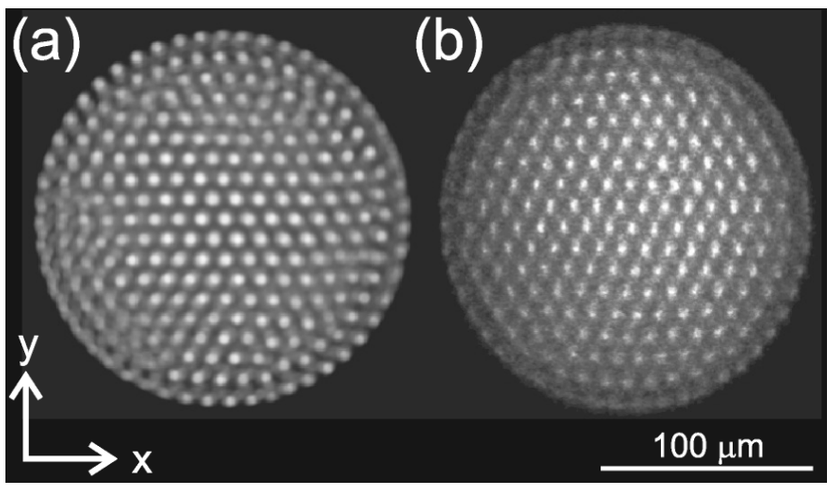

FIG. 3. Images of Coulomb crystals. (a) Time averaged image based on data from MD simulations of Coulomb clusters with 2685 ions at $\Gamma \sim 400$ (temperature: $\sim$5 mK). The averaging time is 10 ms. (b) Image from experiments with clusters containing $\sim$2700 ions.

A. Mortensen et al.,
Phys. Rev. Lett. 96, 103001 (2006)

Coherent control of the ion motion

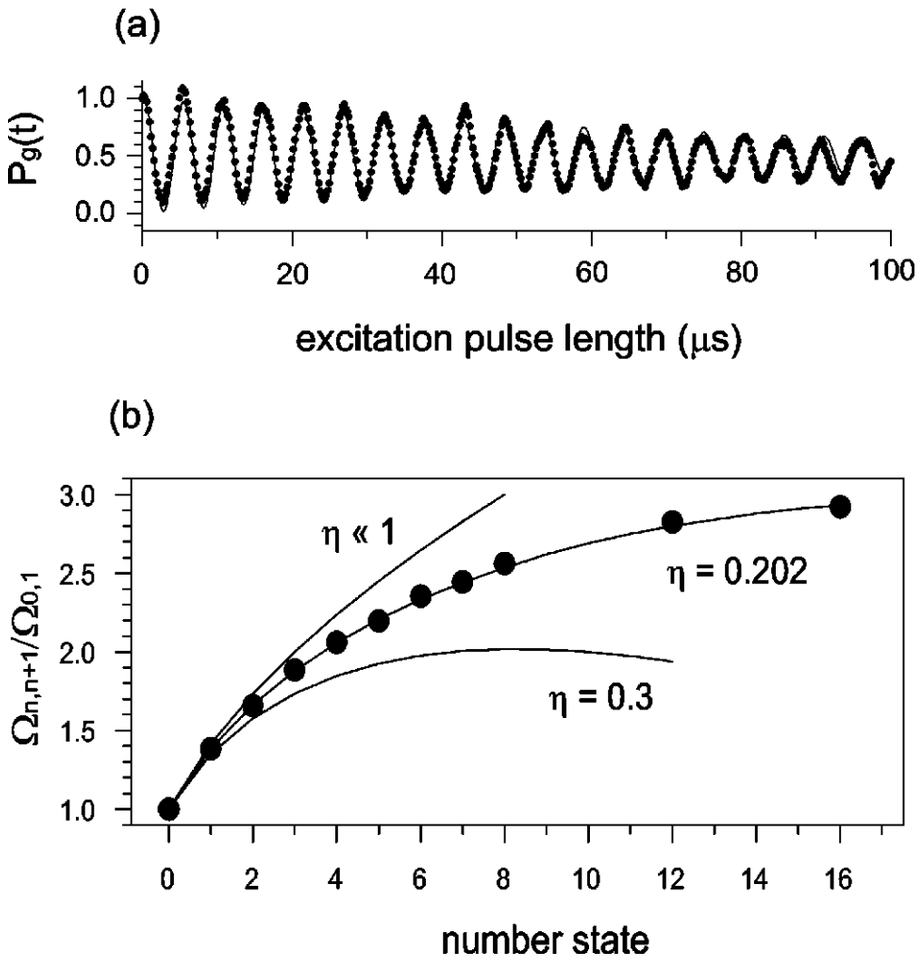

FIG. 11. Number states in the NIST experiment (Meekhof *et al.*, 1996): (a) Rabi oscillations on the blue sideband for the ground state in the trap ($n=0$); (b) ●, measured ratio of Rabi frequencies for different number states; solid lines, theoretical predictions for several Lamb-Dicke parameters.

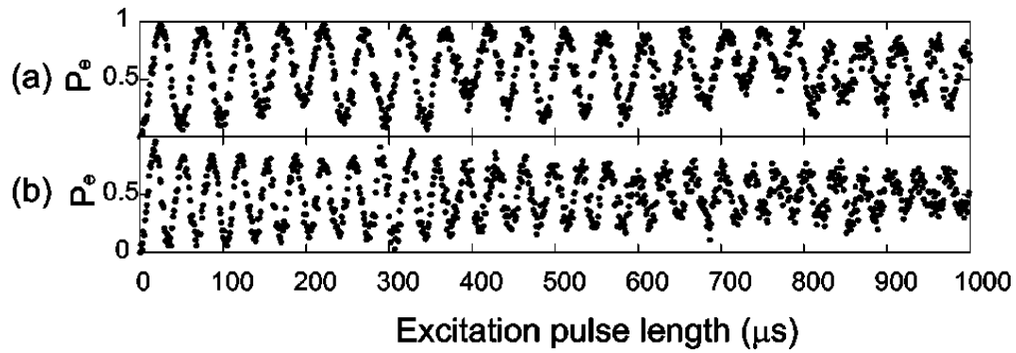

FIG. 12. Number states in the Innsbruck experiment (Roos *et al.*, 1999): (a) Rabi oscillations on the blue sideband for the ground state ($n=0$); (b) Rabi oscillations as in (a) but now for the number state $|n=1\rangle$.

Dehmelt, Paul and Wineland

The Nobel Prize in Physics 1989

Norman F. Ramsey
Prize share: 1/2

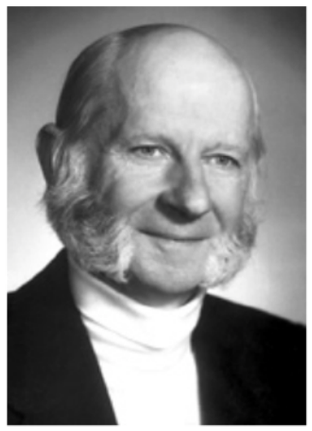

Hans G. Dehmelt
Prize share: 1/4

Wolfgang Paul
Prize share: 1/4

The Nobel Prize in Physics 1989 was divided, one half awarded to Norman F. Ramsey *"for the invention of the separated oscillatory fields method and its use in the hydrogen maser and other atomic clocks"*, the other half jointly to Hans G. Dehmelt and Wolfgang Paul *"for the development of the ion trap technique"*.

The Nobel Prize in Physics 2012

Photo: U. Montan
Serge Haroche
Prize share: 1/2

Photo: U. Montan
David J. Wineland
Prize share: 1/2

The Nobel Prize in Physics 2012 was awarded jointly to Serge Haroche and David J. Wineland *"for ground-breaking experimental methods that enable measuring and manipulation of individual quantum systems"*

Light & Matter (part 2)

Cavity quantum electrodynamics

Vacuum Rabi oscillations

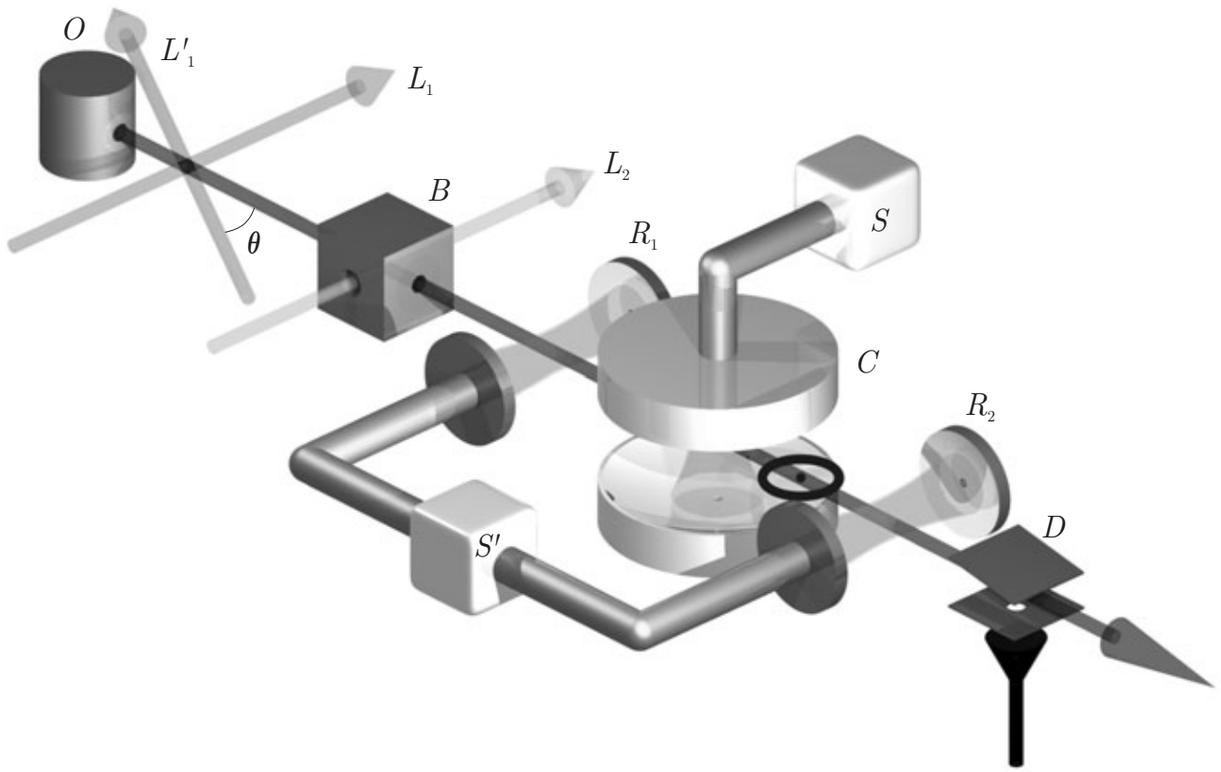

Fig. 5.15 General scheme of the CQED experiments with circular Rydberg atoms.

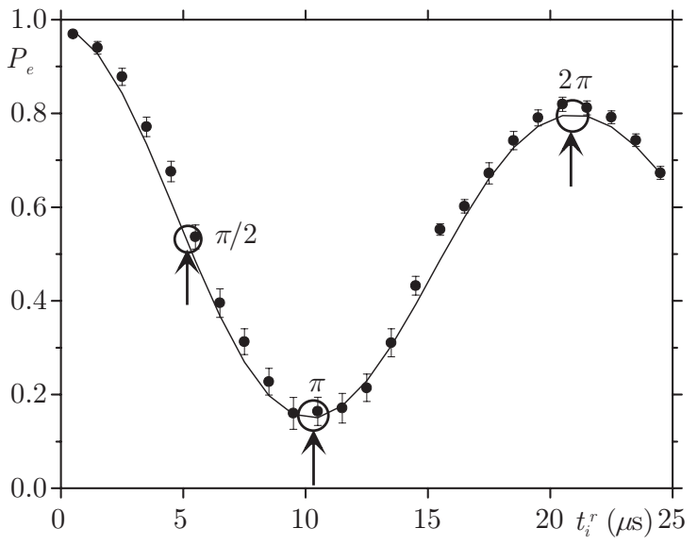

Fig. 5.29 Important atom–cavity interaction times in the vacuum Rabi oscillation. First period of curve (A) in Fig. 5.26 with $\pi/2$-, π- and 2π-quantum Rabi pulses highlighted. Reprinted with permission from Brune *et al.* (1996b). © American Physical Society.

Haroche & Raymond, *Exploring the Quantum*, Oxford

Single-photon pistol

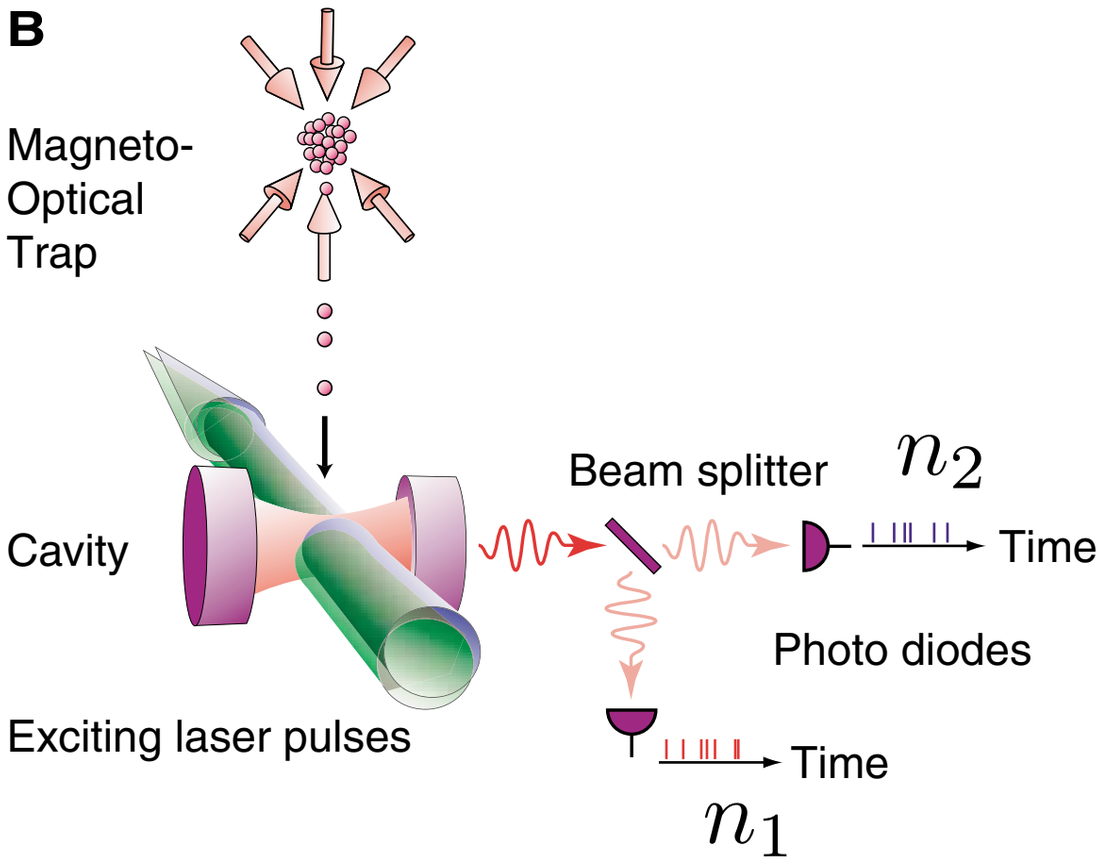

$$g^{(2)}(\tau) = \frac{\langle n_1(t) n_2(t+\tau) \rangle}{\langle n_1(t) \rangle \langle n_2(t+\tau) \rangle}$$

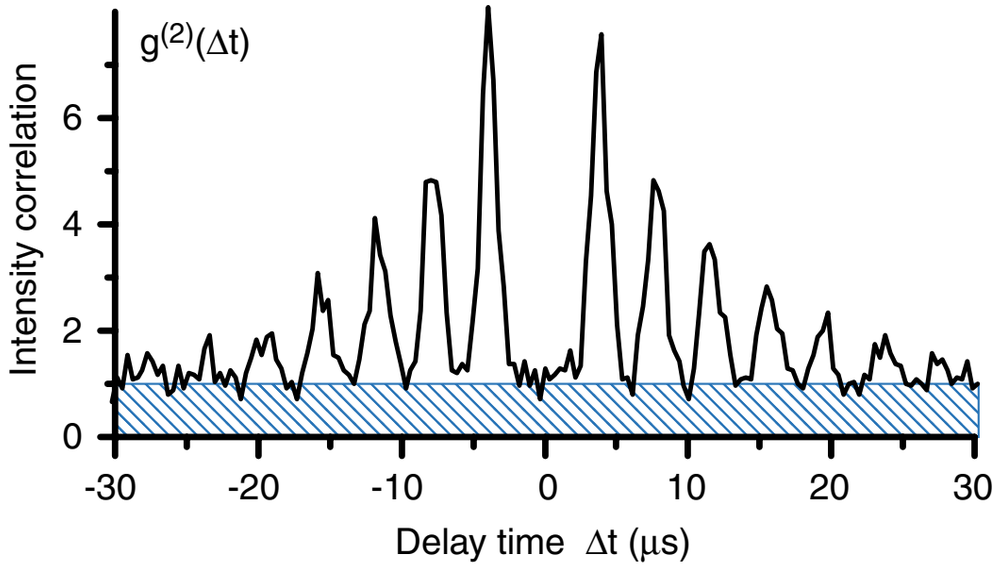

FIG. 4 (color online). Second-order intensity correlation of the emitted photon stream, averaged over 15 000 experimental cycles (loading and releasing of the atom cloud) with a total number of 184 868 photon counts. The hatched area represents correlations between photons and detector-noise counts.

A. Kuhn et al., Phys. Rev. Lett. 2002

Dynamics induced by an arbitrary state in the cavity

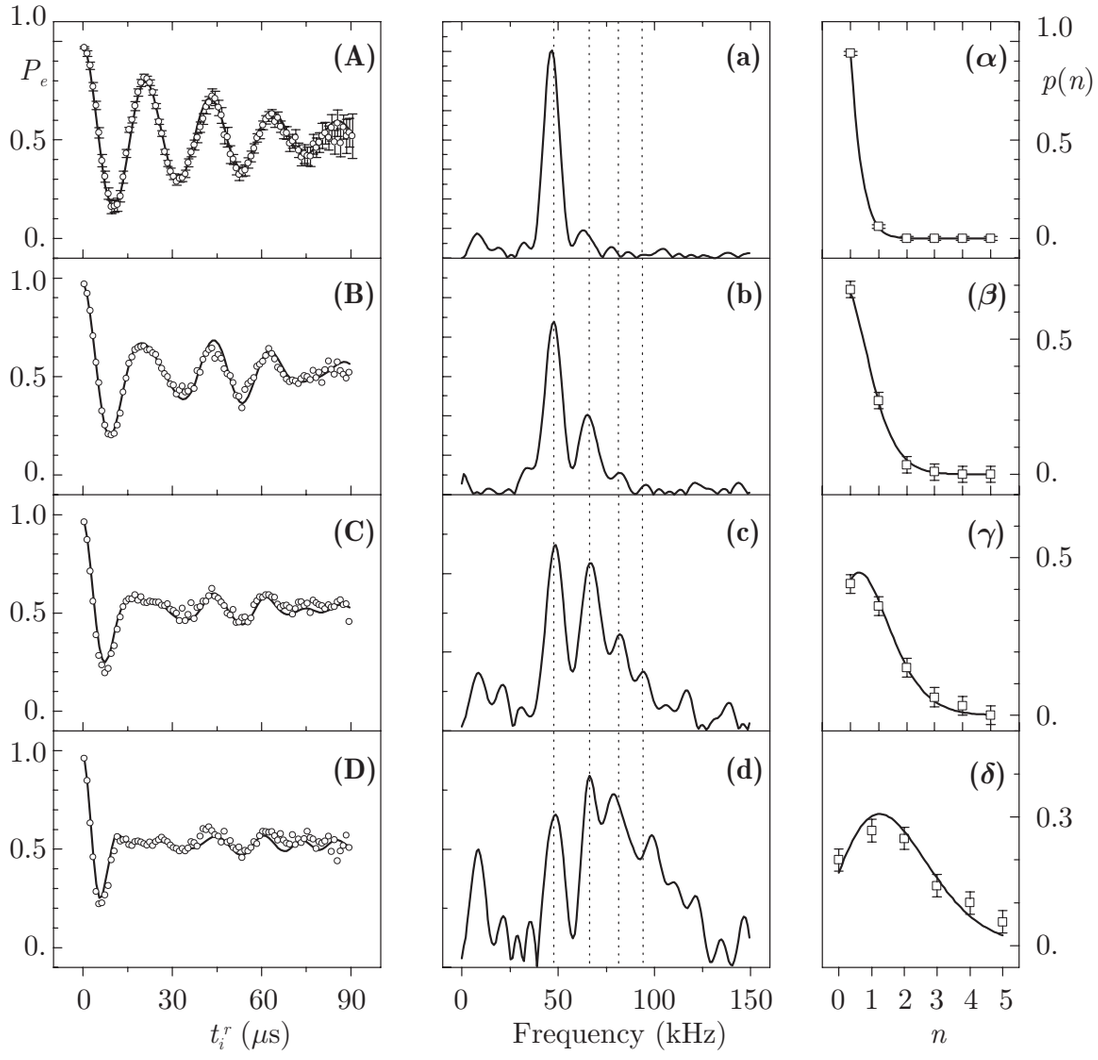

Fig. 5.26 Rabi oscillation in a small coherent field. (A), (B), (C) and (D): Rabi signal representing $P_e(t_i^r)$, for fields with increasing amplitudes. (A): no injected field (B), (C) and (D): coherent fields with 0.40 ($\pm$0.02), 0.85 ($\pm$0.04) and 1.77 ($\pm$0.15) photons on average. The points are experimental [errors bars in (A) only for clarity]; the solid lines correspond to a theoretical fit. (a), (b), (c), (d): corresponding Fourier transforms. Frequencies $\Omega_0/2\pi = 47$ kHz, $\sqrt{2}\Omega_0/2\pi$, $\sqrt{3}\Omega_0/2\pi$ and $2\Omega_0/2\pi$ are indicated by vertical dotted lines. Vertical scales are proportional to 4, 3, 1.5 and 1 from (a) to (d). (α), (β), (γ), (δ): Photon number distributions $p(n)$ inferred from the experimental signals (points). Solid lines show the theoretical thermal (α) or coherent [(β), (γ), (δ)] distributions which best fit the data. The inferred residual thermal photon number is $n_{\rm th} = 0.06$ for (A). Reprinted with permission from Brune *et al.* (1996b). © American Physical Society.

Haroche & Raymond, *Exploring the Quantum*, Oxford

Vacuum Rabi splitting

85Rb atom in a cavity

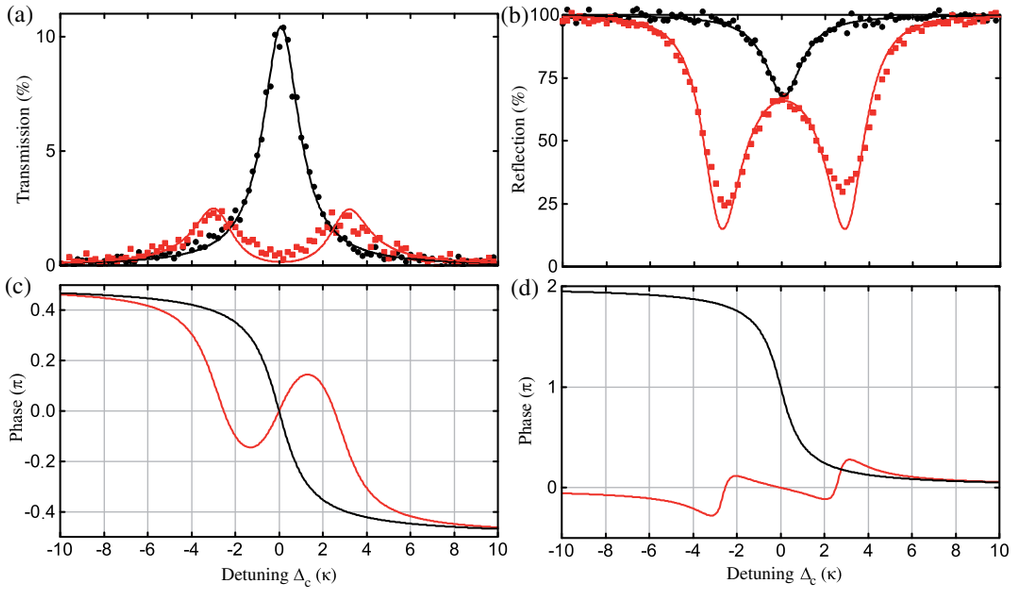

FIG. 6 (color online). (a) Transmission and (b) reflection spectra of a single-sided, overcoupled cavity in the strong-coupling regime. Without the presence of an atom (black circles and black fit curves), the cavity exhibits a Lorentzian transmission resonance, which is also observed as a drop in reflection. The sum of transmission and reflection is less than 100% due to mirror absorption and scattering. With an atom trapped in the mode (gray squares and gray theory curves), the vacuum-Rabi peaks are clearly resolved. The discrepancy of the data points from the theory curve is explained by inhomogeneous broadening of the atomic transition frequency. (c), (d) Phase response in the coupled (gray) and uncoupled (black) cased in (c) transmission and (d) reflection. On resonance, a phase shift of π is observed in reflection for the case of an empty cavity.

A. Reiserer & G. Rempe, Rev. Mod. Phys. 2015

Superconducting qubit in a cavity

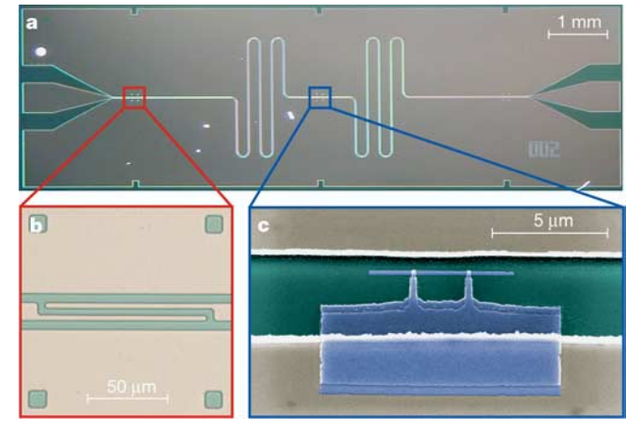

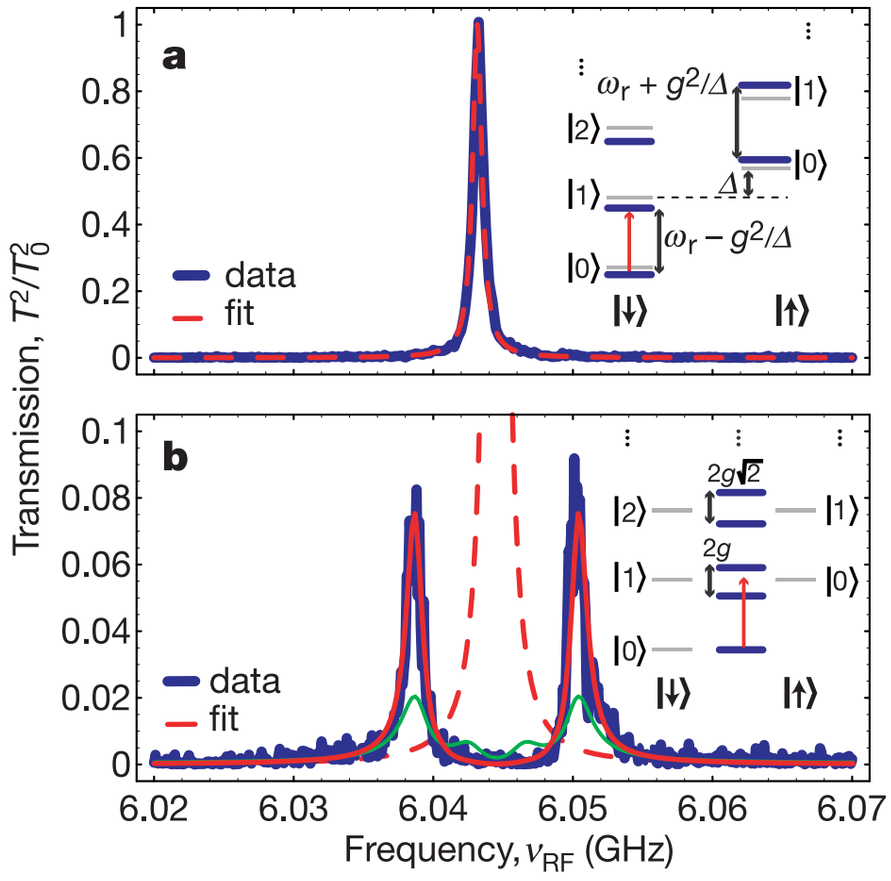

A. Wallraff et al., Nature 2004

Photon blockade

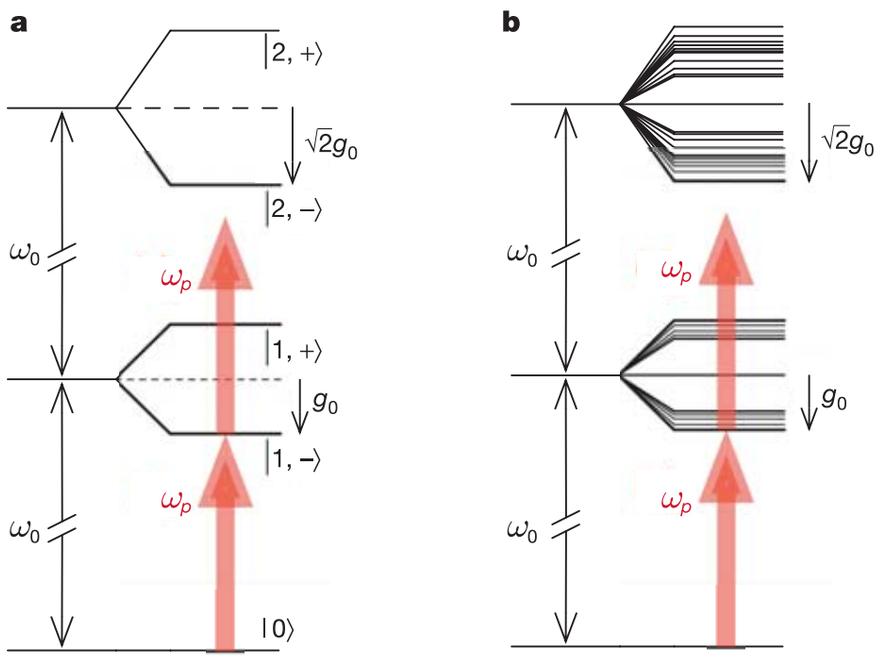

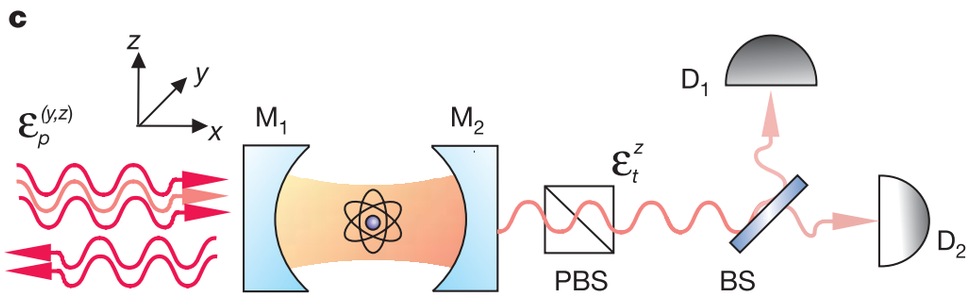

Figure 1 | The atomic level structure used for implementation of the photon blockade effect, and a simple diagram of the experiment. **a**, Atomic level diagram showing the lowest-energy states for a two-state atom of transition frequency ω_A coupled (with single-photon Rabi frequency g_0) to a mode of the electromagnetic field of frequency ω_C, with $\omega_A = \omega_C \equiv \omega_0$ (ref. 15). Two-photon absorption is suppressed for a probe field ω_p (arrows) tuned to excite the transition $|0\rangle \rightarrow |1,-\rangle$, $\omega_p = \omega_0 - g_0$, leading to $g^{(2)}(0) < 1$ (ref. 13). **b**, Eigenvalue structure for the $(F = 4, m_F) \leftrightarrow (F' = 5', m_F')$ transition coupled to two degenerate cavity modes $l_{y,z}$, as discussed in the Supplementary Information. Two-photon absorption is likewise blocked for excitation tuned to the lowest eigenstate (arrows). **c**, Simple diagram of the experiment. BS, beam splitter.

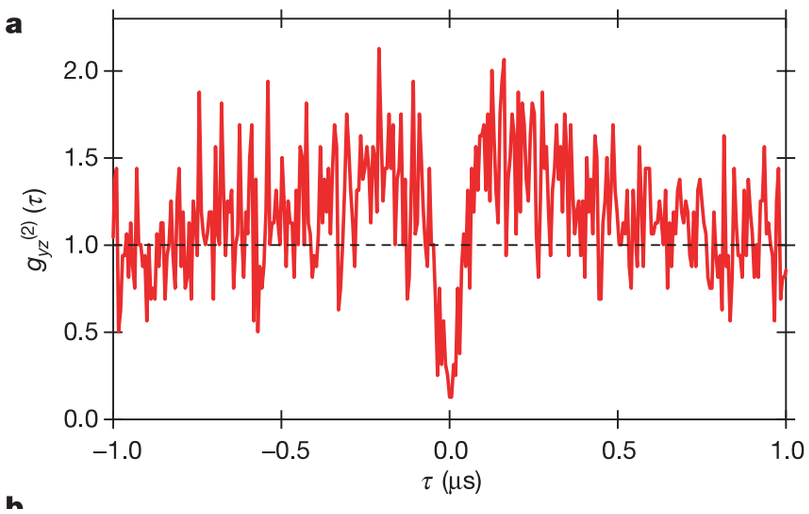

Figure 3 | Experimental measurements of the intensity correlation function $g_{yz}^{(2)}(\tau)$ for incident excitation with polarization along $\hat{y}$ and detection with orthogonal polarization $\hat{z}$. **a**, $g_{yz}^{(2)}(\tau)$ over the interval $|\tau| \leq 1.0\,\mu s$ demonstrates that the transmitted field exhibits both subpoissonian photon statistics $g_{yz}^{(2)}(0) = (0.13 \pm 0.11) < 1$ and photon antibunching $g_{yz}^{(2)}(0) < g_{yz}^{(2)}(\tau)$ (ref. 17). **b**, $g_{yz}^{(2)}(\tau)$ over longer intervals $|\tau| \leq 10\,\mu s$ displays a pronounced modulation due to axial motion of the trapped atom. **c**, The Fourier transform $\tilde{g}(f)$ of $g_{yz}^{(2)}(\tau)$ with the independently determined minimum and maximum frequencies ν_{min} and ν_0 for axial motion in a FORT well indicated by the dotted lines. $g_{yz}^{(2)}(\tau)$ is plotted with 6-ns resolution in **a** and with 12-ns resolution in **b**.

Birnbaum et al., Nature 2005

Quantum optics and Nobel prizes: Glauber & Haroche

The Nobel Prize in Physics 2005

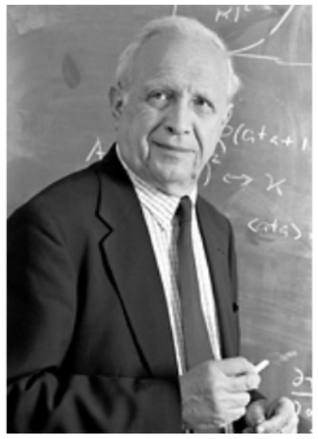

Photo: J.Reed
Roy J. Glauber
Prize share: 1/2

Photo: Sears.P.Studio
John L. Hall
Prize share: 1/4

Photo: F.M. Schmidt
Theodor W. Hänsch
Prize share: 1/4

The Nobel Prize in Physics 2005 was divided, one half awarded to Roy J. Glauber *"for his contribution to the quantum theory of optical coherence"*, the other half jointly to John L. Hall and Theodor W. Hänsch *"for their contributions to the development of laser-based precision spectroscopy, including the optical frequency comb technique"*.

The Nobel Prize in Physics 2012

Photo: U. Montan
Serge Haroche
Prize share: 1/2

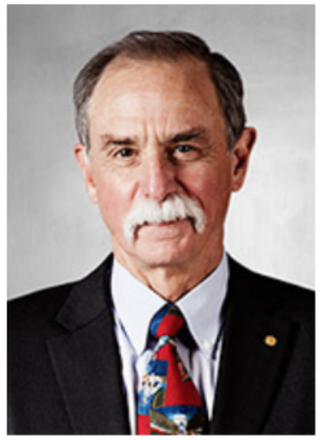

Photo: U. Montan
David J. Wineland
Prize share: 1/2

The Nobel Prize in Physics 2012 was awarded jointly to Serge Haroche and David J. Wineland *"for ground-breaking experimental methods that enable measuring and manipulation of individual quantum systems"*